

DESIGN AND FABRICATION OF A BISTABLE UNIT ACTUATOR WITH MULTI-MATERIAL ADDITIVE MANUFACTURING

T. Chen , J. Mueller , K. Shea

Engineering Design and Computing Laboratory
Department of Mechanical and Process Engineering
ETH Zurich, Zurich, 8092, Switzerland
ttc · jm · kshea @ ethz . ch

Abstract

Bistable systems have two stable equilibrium states around which they can be perturbed. Bistability in a mechanical system requires large deformation, which is commonly accommodated by means of springs or soft joints. In this paper, the authors leverage the ability of advanced Additive Manufacturing (AM) technology that enables printing of materials of varying stiffness values to design and fabricate monolithic bistable unit actuators that maximize the stroke length. A Von Mises Truss (VMT) based bistable structure utilizing snap-through buckling behavior is designed and fabricated. By varying the material stiffness and length of the joints, the authors are able to adjust the activation forces while keeping the geometry constant. 56 specimens are fabricated and tested in tension and compression. Numerical simulation models are constructed and the results are found to correlate well with experimental data. The required activation force can be increased with a decrease in joint length or an increase in joint material stiffness.

Introduction

Active structures have received increasing attention in response to new engineering challenges such as unfamiliar and changing environments [1], but also as a new venue for architectural and artistic expression [2]. The need for such structures arises from two broad categories, one where controlled periodic state change is desirable. Examples include robotic manipulators, active building facades, HVAC systems, and large scale space structures [3]. Other category features structures where the change typically occurs once and must be “reset” after. Examples in this category include energy absorbers [4] and gripping and trapping concepts such as an artificial Venus flytrap [5].

As summarized by Korkmaz [1], a typical active structure requires constant power input to remain stable, and must be geometrically accurate and possess structural integrity to carry the designed loads. Multi-material Additive Manufacturing (AM) technologies have been utilized to fabricate active structures. Ge et al. [6] utilized the shape memory effect of printed polymers to “lock-in” pre-stress, and achieve shape change through temperature variation. Tibbits [7] achieved large displacement and configuration changes through swelling of a hydrogel based material also

printed with the same AM technology. However, neither approaches offer predictable structural integrity, and lack the permanence and controllability required by a typical active application.

Bistability is a buckling-induced mechanical phenomenon that has been increasingly exploited to achieve structural form and functional change [8]. As a bistable structure possesses two equilibrium states, input energy is only needed to transform the state of the structure and not to maintain such a state [9]. Since both the stroke length and the state transitioning force are defined, accurate activation and load bearing capability is inherent in such a structure.

In this work, the authors design, fabricate and test a reversible bistable unit actuator that can be fabricated with a multi-material 3D printer monolithically. The goals of the design are to achieve multiple stable states while maximizing the stroke length and allowing the activation force to be adjustable and predictable. It is uniquely designed for a multi-material fabrication process. As the 3D printer is able to deposit materials with varying Young's Moduli, the authors tailor the stiffness and the dimension of the joints to allow the bistable actuator to activate with a range of forces without changing its overall geometry. Lastly, the design is fabricated as small as possible to encourage multi-actuator designs that form larger structures.

This paper starts with background on bistable mechanisms, the particular AM technology used and joint designs. The following section details an investigation on the printed materials and proposes stress strain relationships for each. Then the geometry of the proposed bistable actuator is described, following with its simulation and validation with physical experiments. A discussion and conclusion follows.

Background

This work combines a bistable mechanism with a multi-material 3D printer to design and fabricate a bistable actuator that achieves the goals set out in the introduction. This section first discusses previous fabrication of bistable mechanisms, then provides the theoretical knowledge necessary for the design of a 3D printed multi-material bistable unit actuator. Lastly the implication of the joint fabrication methods are discussed in relation with the multi-material printing technology.

Design and Fabrication

A bistable structure has two stable equilibrium configurations. After a small force perturbation, the structure returns to the initial configuration, similar to a static structure. When the perturbation reaches the magnitude of the activation force, the system suddenly snaps to the second stable equilibrium. This follows from the sudden large deformation behavior observed when a structure buckles. Bistable phenomenon is exhibited in certain four bar linkages [10], and with limit point buckling based designs such as the Euler buckling beam [11] and the Von Mises Truss (VMT) [12].

Euler buckling type bistability consisting of a single beam curved in its first buckling mode is popular in literature due to its ease-of-fabrication and large stroke length [13]. Researchers have used such a design as an acoustic damper [14] and energy absorber [15]. The quad-stable structure

proposed by Han et al. [16] focused on the rigidity of the frame constraining the buckling elements. Oh and Kota [17] proposed a flat design and stated that single layer monolithic fabrication reduces time and material consumption. Restrepo [15] presented the first study of combining the Polyjet printing technology with the fabrication of multi-stable structures, albeit still with a single material. These concepts are adopted and further developed in this work.

Bistability with Von Mises Trusses

Another class of bistable actuators exploits the limit point buckling behavior where two unbuckled bars snap to another equilibrium state under a force that is infinitesimally greater than the activation force. Von Mises proposed such a bistable structure in 1923 [12]. A VMT (see Fig. 1a) consists of two truss bars pin jointed at the apex and at the supports. VMT exhibits limit-point buckling, where load increase beyond the critical point would change the structural configuration (Fig. 1b). If the vertical load F is applied at the apex and w is the downward displacement from a line drawn between the supports, the relationship between F and w follows Eqn. (1), where E and A are the material stiffness and the cross sectional area of the bars respectively.

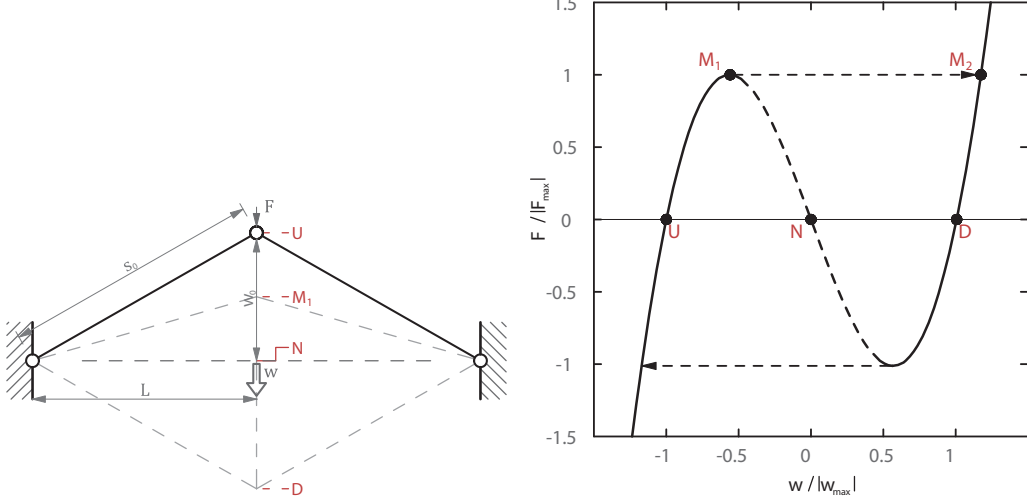
$$F = -EA\left(\frac{1}{w^2 + L^2} - \frac{1}{w_0^2 + L^2}\right)w \quad (1)$$

With Eqn. (1), one can plot the load displacement curve (Fig. 1b); the same critical points that exemplify bistability are shown in both figures (Fig. 1a and 1b). Points U and D are the equilibrium states when the load F is zero. M_1 is the critical point at which an infinitesimal increase in load triggers instability. With the increase in load, the structure snaps, upon which the VMT essentially mirrors itself along the horizontal axis. With a further increase in load, the bars experience tension and eventually rupture. If the load is displacement controlled, past point M_1 , the reaction force decreases and eventually reverses orientation past point N and reaches a maximum between point N and D .

Joint Construction

Unlike the Euler bistability design where the whole beam undergoes deformation, the idealized VMTs assume that the truss bars are connected to the bracket with idealized pin joints. In the fabricated design however, the joints must be able to accommodate the large and repeated rotation. Schioler and Pellegrino designed a VMT based device [3] constructed with Nylon injection molding. The members are thinned at the joints and behave as a live hinge. A micro adoption of VMT is used for energy absorption [18], where the material is uniformly flexible.

In this work, the authors aim to design and fabricate an actuator such that the stroke to span $|w_0|/L$ ratio is as large as possible, and therefore the members in such a design are already at the lower limit of the fabrication resolution. An alternative joint solution is proposed whereby the design utilizes joints with the same cross section but lower stiffness values. This simulates the behavior of a typical joint where the thinning region is replaced by a region where the stiffness is proportionally lower.



(a) A VMT consisting of two truss bars with geometrical variables labeled (b) Load displacement curve of a typical VMT according to Eqn. (1)

Figure 1: Configuration and load displacement curve of a VMT, critical points are labeled.

Material Study

The proposed design relies on a fabrication process that can produce materials of different stiffness values. The Stratasys Objet500 Connex3 achieves this by depositing and mixing liquid photopolymers from an array of nozzles in a layer by layer fabrication process. UV light cures the recently printed layer before the print platform lowers and the next layer is printed. This allows the different materials to be assigned to any region of a design.

With this 3D printer, available stiffness values are not a continuous variable. Rather the printer allows the mixing of two or more base materials in 12 discrete steps, yielding 14 different material combinations for each pair. Of particular interest are the mixtures between TangoBlack+ (TB+), an elastomer-like material, and VeroWhite+ (VW+), a rigid plastic to create 12 intermediate digital materials (DMs) of varying stiffness values.

The material manufacturer provides the Young's Modulus and fracture strain for the seven DMs on the rigid end of the spectrum but not for the flexible ones. Stanković et al. [19] presented the Young's Modulus of all 14 materials, showing large deviations from the manufacturer's specification and the stress-strain relationships were not included. The deviations were attributed partly to unknown test conditions [20]. As bistability entails large deflection [21] and finite strain behavior of the elastomers, quasi-static tensile tests are conducted under constant environmental conditions in this study. The results are used in the simulation models that predict the behavior of the unit actuators.

Method

This section describes the proposed bistable actuator and shows that the actuator achieves the goals described in the introduction. Namely, the proposed bistable actuator possesses two

equilibrium states and is reversible; that the actuator can be fabricated monolithically with a 3D printer and have predictable activation force that can be tailored through joint length and material change. Lastly, the stroke length is maximized while keeping the design as small as possible.

To demonstrate bistability as well as predictability of the activation force, first a material characterization is performed to determine the mechanical properties of the printer materials. Second, a parametric study is conducted both with numerical simulation and with physical experiments on 56 specimens of varying joint length and joint material.

Unit Actuator Design

The proposed bistable actuator shown in Fig. 2 originates from the VMT scheme. The physical realization requires rigidity laterally and out of plane. As suggested in [3] and [22], the side-way movement is restricted by stacking two VMTs vertically, and the out-of-plane movement is restricted by increasing the depth of the entire actuator. In using such an actuator as a unit, and to maximize the stroke length, the design must be self-contained and small. This places an emphasis on the design of the flexible joints critical to VMTs. It was stated that compared to an Euler buckling based bistable mechanism, the stroke distance provided by VMTs is much smaller [3]. To overcome this limitation, the proposed actuator provides a $|w_0|/L$ ratio of 1 where w_0 and L are the width and the height of the actuator respectively. This effectively allows the stroke length, s , to double the actuator height $s = 2w_0$.

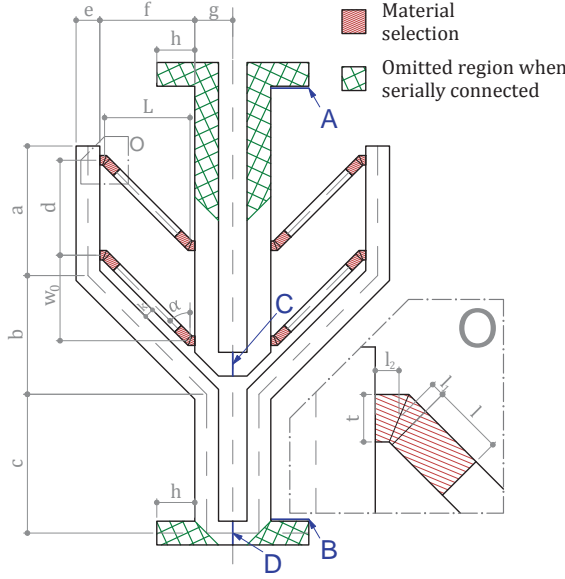


Figure 2: Design of the integral bistable actuator unit showing the retracted state as well as the design parameters.

Table 1: Design parameters defining the actuator design on the left. The joint length, l , is a variable and is subject to the parametric study in the following section.

Parameter	Value	Parameter	Value
a	6.825 mm	w_0	4.50 mm
b	6.250 mm	L	4.50 mm
c	6.675 mm	l_1	0.15 mm
d	5.00 mm	l_2	0.25 mm
e	1.25 mm	l	0.75 mm
f	5.00 mm	t	0.50 mm
g	2.00 mm	k	0.50 mm
h	2.00 mm	α	45°

The design consists of a bracket, four truss bars and a pin. The bracket, the pin and the center portion of the truss bars are fabricated with VW+, and are much stiffer than the joints indicated

by the line-hatched regions. The design is dimensioned so that the smallest elements coincide with the precision of the fabrication method. Note that the bracket cannot be assumed to be rigid as its flexibility partly allows the actuator to function. All variables are listed in Table 1. The joint geometry is created such that it is perpendicular to both the bracket and the pin to ensure the contact area remains constant and does not depend on the inclination angle, α . The cross-hatched regions indicate the additional parts included to facilitate tensile testing. When removed, one notes that the bottom of the bracket has the same geometry as the pin. Therefore, when many actuators are stacked together in series, the total extended length nearly doubles the retracted length.

The design is assumed to be rigid in the out-of-plane direction and has a thickness of 4 mm. The angle of inclination of the truss bars, $\alpha = \tan(w_0/L)$, is set to 45°. The stroke length, $2w_0$, is dependent on the inclination angle. The minimum spacing of the fabrication process k dictates how close two features may be placed without being fused together. The extrusion of length h is added to the design for simulation and testing purposes to maintain a predictable load condition across all specimens. It is important to note that the extrusions on the pin and on the brackets are in line with each other and therefore no applied moment is generated. The line-shaded region indicates the location of the joint and a change in material stiffness. Parameter l defines the length of the joint and is specified in the parameter study section. Note that changing l does not change the overall geometry, i.e. if the joint lengthens, the truss itself shortens.

Printer Material Characterization

To adequately simulate, as a part of the parametric study, the large displacement and strain necessitated by the VMT mechanics, a complete stress-strain model for each joint material must be provided. With the Connex printer, between TB+ and VW+, 12 DMs can be deposited within one print. The last two digits of each material name is its Shore hardness values (Shore A for the six DMs in the first group, and Shore D for the second). The complete set of materials is shown in Fig. 3.

	Base Material	Digital Material					
		F9840	F9850	F9860	F9870	F9885	F9895
Group 1	TB+						
Group 2	VW+	R8505	R8510	R8515	R8520	R8525	R8530

Increase in stiffness

Figure 3: Material table with labels, grouping and base/digital distinction shown. Direction of stiffness increase is indicated.

The following describes the tensile testing procedure that is performed for each material in Fig. 3. Type V geometry of the ASTM D638-10 test standard for tensile testing of plastics is adopted for all specimens. Three identical test specimens are printed for each material under an ambient temperature of 21 °C. To eliminate the impact of uncontrolled factors on the mechanical properties [20], each is printed on a separate tray. Aside from the material combination, all other factors are held constant. Tensile tests are conducted on an Instron ElectroPuls 3000 with either a 100 N or a 5000 N load cell, depending on the material tested. Under displacement control, a testing speed of 20 mm min⁻¹ is set and the specimens are elongated until fracture.

Parametric Design Study

With both the actuator geometry and the material properties defined, a study can be conducted to assess the effect of the joint on the overall behavior and the activation forces. As discussed in the actuator design section, the varying parameters are the geometry and the material of the VMT joints. The printed position, retracted or extended, of the actuator during fabrication is included as an additional parameter. Along with four different joint lengths and seven different joint materials, the parametric variations lead to a total of 56 models. These models are compared with the analytical solution, simulated numerically, and are fabricated. Quasi-static load testing is conducted on the fabricated specimens. Figure 4 shows the different parameters and the corresponding geometry and printed specimens. It is hypothesized that decreases in the joint length or increases in the material stiffness of the joint will increase the activation force.

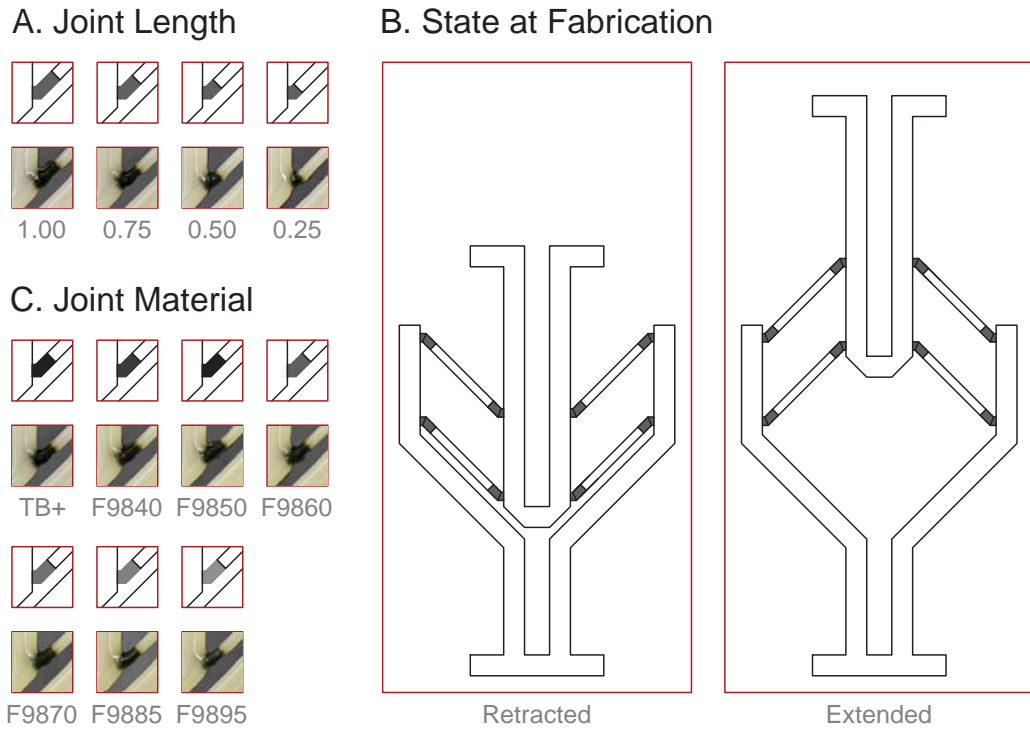


Figure 4: The design parameters including joint length, actuator state at fabrication and joint material investigated in the parametric study are shown by focusing on one joint

Analytical Solution The analytical solution in terms of Eqn. (1) is used for comparison. Two shortcomings are noted in the analytic model. One, a VMT assumes the joints are idealized pins, whereas in the design presented in this work, joints have finite geometry and stiffness. Considering this, the authors propose to substitute E with a modified Young's Modulus assuming each truss is a series of connected springs of varying stiffnesses, i.e. E_j represents the stiffness of the joint material.

$$E_{\text{Mod}} = \frac{1}{2\frac{1}{E_j} + \frac{1}{E_{\text{VW+}}}} \quad (2)$$

The second shortcoming is that the bracket is assumed to be rigid in the analytical solution, whereas in reality, they bend as the pin is extended. One potential way to incorporate this effect in the theoretical equation is to add a linear spring in between the supports and assume that the supports are a pin and a roller, and not fully fixed. This will be investigated in a future study.

Numerical Simulation A finite element based simulation is performed to predict the behavior of a unit actuator. With the intent to reduce computational effort rather than a formal finite element comparison as done by Cherry [22], two sets of simulations are implemented. The first aims to replicate both the form and the boundary conditions of a physical actuator (Fig. 5A). As such, brick elements are used to mesh the volume. A finite displacement of 10 mm min^{-1} is applied to surface A of Fig. 2; surface B is pin jointed. Symmetry conditions are imposed on surfaces C and D to reduce computational effort. Material properties summarized in Table 2 are incorporated into each analysis. Since this is a displacement based simulation, a physically and geometrically non-linear analysis is performed without arc-length control.

The second set of simulations assumes that the depth and the width of each section can be approximated as that of a rectangular beam. With that, the model is reduced to a frame and meshed with quadratic Timoshenko beam elements. The beams are placed at the centerline of the solid geometry. Where there is a connecting point between two members, a rigid link is placed to eliminate artificial flexibility (Fig. 5B). The boundary conditions and the material model remain the same as the previous simulation model. With the beam model, each of the parametric variations are numerically simulated.

The focus of this study is not on the eventual failure of the joints. Therefore, the displacement load is restricted between 0 and the stroke length. No failure criterion is set, nor is there a contact condition between the pin and the bracket in the case of compressive displacement with the extended specimens. The solid model is used as a benchmark of the parametric study that uses the beam model. As such, a random case of $l = 0.75 \text{ mm}$ and FLX9860 as the joint material is selected as the benchmark model. Both retracted and extended states are simulated, resulting in two simulation models.

Experimental Validation The aforementioned models are fabricated on the multi-material 3D printer. The surface finishing is set to glossy to ensure that the specimens are not encased by support material. The support material does not dissolve with a solution and must be washed away with a water jet. With delicate specimens, the effect of the water jet must be avoided. The Instron apparatus is used to conduct both tensile and compressive testing. All specimens are tested on the day they are fabricated and no state change occurs prior to testing. To ensure that the boundary conditions remain invariant across all models, a set of two customized grippers are printed to hold the specimens by the protrusions dimensioned h shown in Fig. 2. The grippers themselves remain clamped to the Instron at a pressure of 0.5 MPa. For the retracted specimens, a tensile displacement of 10 mm min^{-1} is set and the specimens are elongated until rupture. For the extended specimens,

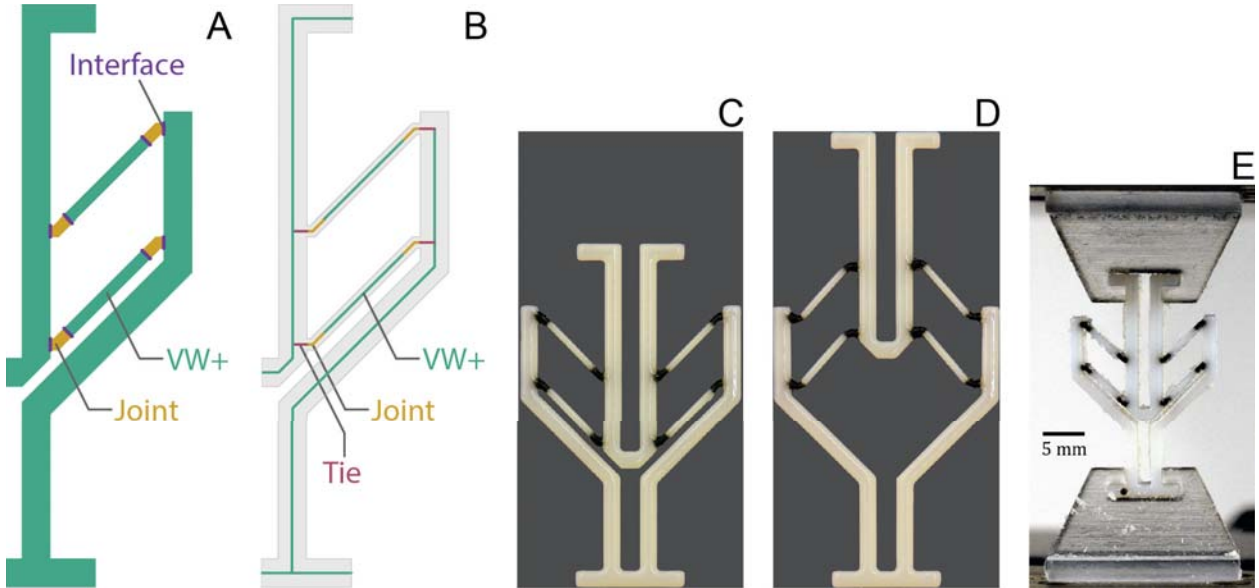


Figure 5: The Solid (A) and Beam (B) FEM model with material and interfaces shown. (C) The benchmark actuator printed in the retracted state, and extended through an applied tensile force (D). The experimental setup showing the grippers (E).

a compressive displacement of equal magnitude is applied. Both the actual displacement and the reaction force are recorded for each specimen.

Results

This section presents both the result from material characterization and that from the parametric study. From the material characterization, first the force displacement curves of each of the 14 materials are shown. Then a multi-linear elastoplastic constitutive model is constructed for each material to be used in the numerical simulation. From the parametric study, the validity of the theoretical model and of the two simulation models are compared using the benchmark specimen (i.e. joint material - F9860 and joint length - 0.75 mm). Then results from the beam model are compared to the physical experiments. Lastly, the activation force required by each specimen is investigated.

Material Characterization

From the exhibited behavior (Fig. 6), the two dominating materials of the mixing process, TB+ and VW+ can be distinguished. Qualitatively, materials printed with TB+ as the base fail slowly, whereas specimens printed with VW+ as the base exhibit necking and fail subsequently from brittle fracture. From material TB+ to VW+, the strength gradually increases, whereas the fracture strain decreases. In the first group (TB+ to F9895), the fracture strain ranges from 30 % to 174 % and ultimate strength ranges from 0.86 MPa to 10.6 MPa. In the second group (R8530 to VW+), the fracture strain ranges from 8 % to 14 % and ultimate strength ranges from 54 MPa to 69 MPa. In general, the observed properties of the DMs can be grouped around the properties of

the two base materials, creating a gap in printable material properties in between.

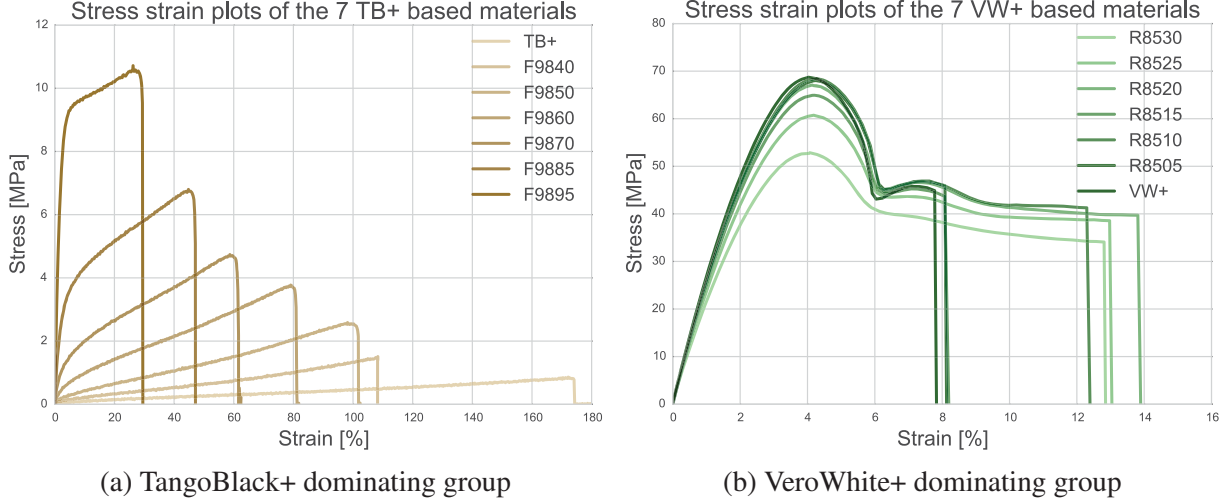


Figure 6: Experimental results showing stress strain curve of each printer material.

This bi-modal distribution of the material properties validates the assumption that the mixed materials' properties depend heavily on the base material used. Attention is focused on the TB+ dominating group where the allowable strains are deemed sufficient to accommodate the large deformation induced by the snapping behavior and the range of allowable stresses are sufficient to deliver the desired activation forces. To simplify the material behavior, each of the 7 TB+ based materials is assumed to be able to be adequately modeled by a tri-linear stress strain relationship. The elastic Young's Modulus of each material can be calculated by dividing the first stress by the first strain of that material. The control points of each of the material are listed in Table 2.

Table 2: Constitutive model of materials TB+ to F9895 and VW+ for physically non-linear FEM analyses.

Name	E_{nom} MPa	σ_1 MPa	ϵ_1 -	σ_2 MPa	ϵ_2 -	σ_3 MPa	ϵ_3 -
TB+	0.486	0.850	1.75	-	-	-	-
F9840	1.36	1.50	1.10	1.50	2.00	-	-
F9850	2.65	2.65	1.00	2.65	2.00	-	-
F9860	22.5	0.45	0.02	0.75	0.05	4.0	0.85
F9870	52.5	1.00	0.02	1.60	0.05	4.8	0.60
F9885	125	2.50	0.02	3.75	0.05	7.0	0.45
F9895	375	7.50	0.02	9.50	0.05	10.5	0.26
VW+	2500	50.0	0.02	70.0	0.04	65.0	0.05

Table 2 shows that TB+ can be described by a linear relationship. F9840 and F9850 can be described bi-linearly; the strain value at the first control point of these materials, 200 %, are much higher than that of the stiffer materials. F9860 to F9895 are described tri-linearly, the second strain

point is set at 5 % to describe the softening effect and the third strain point is set at rupture. The behavior of VW+ is distinct from the rest as it belongs to the rigid material group and follows the behavior shown in Fig. 6b.

Analytical and Numerical Models

For the benchmark case, with the geometric data from Table 1 and the material data from Table 2, we obtain the idealized curve in Fig. 7. In the same figure, the force displacement curve of both initial states and of both numerical models are shown. From the figure, bistable behavior can be seen in all models. However, the analytic model presents a symmetric bistable behavior, whereas the numerical models of the actual design show an asymmetric behavior. The stable equilibrium positions are indicated with \otimes , and the unstable ones with \times . Qualitatively similar results have been presented in literature [22]. The actual stroke length is shorter than intended as the force is not zero at the fully extended state ($w = \pm 4.5$ mm). Rather, the curve crosses the zero force line at approximately 2.5 mm for the retracted initial position and -3.0 mm for the extended one, giving the actuator a stroke length of 7 mm and 7.5 mm respectively. Comparing between the solid and the beam numerical models of the retracted state, the behavior is similar. This is in contrast with [22] where it was concluded that the 3D model offered closer agreement due to out-of-plane effects not captured with a 2D model. With respect to the analytic model, the differences in the activation force is 8.8 % for the beam model and 20 % for the solid model. The same observation is made in the extended state, except the differences are greater for the activation force, 55 % and 89 % for the beam and the solid model respectively.

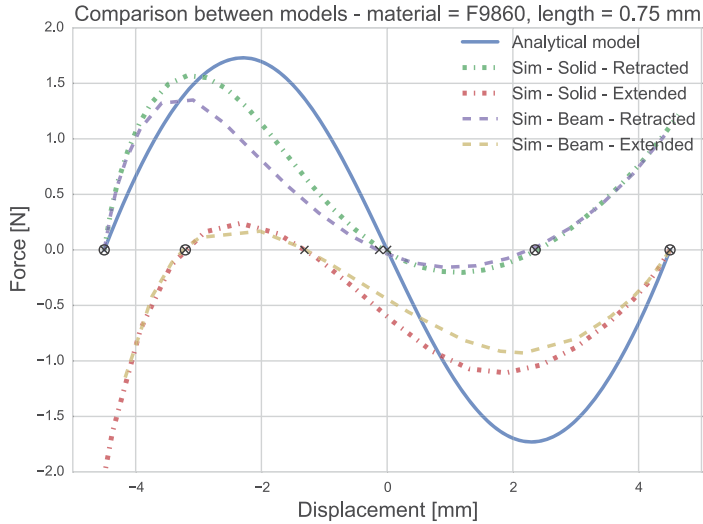


Figure 7: Plots comparing the analytical solution, and simulation featuring solid or beam elements for both retracted and extended initial positions

Beam Model and Experiment Results

As it is difficult to figuratively show the results of all 56 models, plots are made in which only one parameter varies. First, the effect of joint length is investigated by keeping the joint material fixed (Fig. 8). The lengths studied are 1.0, 0.75, 0.50, 0.25 mm (Fig. 4), however during the experiment $l = 0.25$ mm consistently ruptures while undergoing state change. Therefore, designs with such a length are excluded.

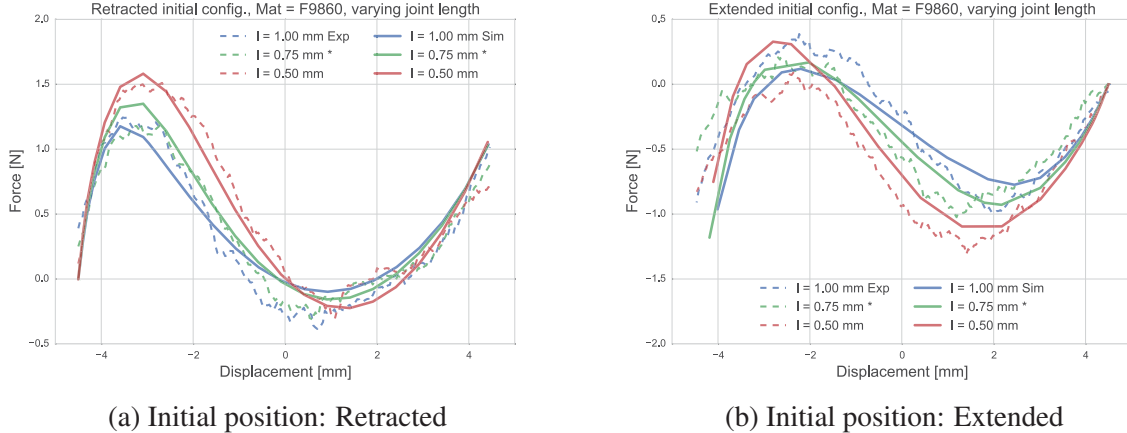


Figure 8: Force-displacement behavior from experiments and simulation with fixed joint material stiffness and varying joint length, * denotes the benchmark configuration

For the retracted initial state, the behavior between experimental data and simulation show remarkable similarity, with a root-mean-square deviation(RMSD) equal to 0.156, 0.115, 0.121 for joint lengths 1.0, 0.75, 0.50 mm respectively. With the initial state being extended (Fig. 8b) the general observations are the same as above. The RMSD of joint lengths 1.0, 0.75, 0.50 mm are 0.402, 0.425, 0.249 respectively.

The second set of figures (Fig. 9) keep the length at $l = 0.75$ mm while varying the joint material from TB+ to F9895. Predictable bistable behavior is observed as the activation force increases with increasing joint stiffness. The discrepancy between simulation and experiment increases at the extremes of joint material stiffness and lessens at the center, with RMSD equal to 0.213, 0.174, 0.143, 0.115, 0.227, 0.479, 0.703 for the retracted initial position and 0.682, 0.649, 0.533, 0.235, 0.363, 0.562, 0.851 for the extended case.

Figures 8 and 9 present results from 18 of the 56 specimens (note that designs where the joint length is 0.25 mm are omitted so the number of useable specimens is 42). The same qualitative observations can be made with the remaining specimens and are omitted here. The important quantitative results are presented below.

Activation Force

As the unit actuator intends to provide varying activation force by changing material parameters, the spectrum of achievable activation forces is plotted in Fig. 10 for both simulation and

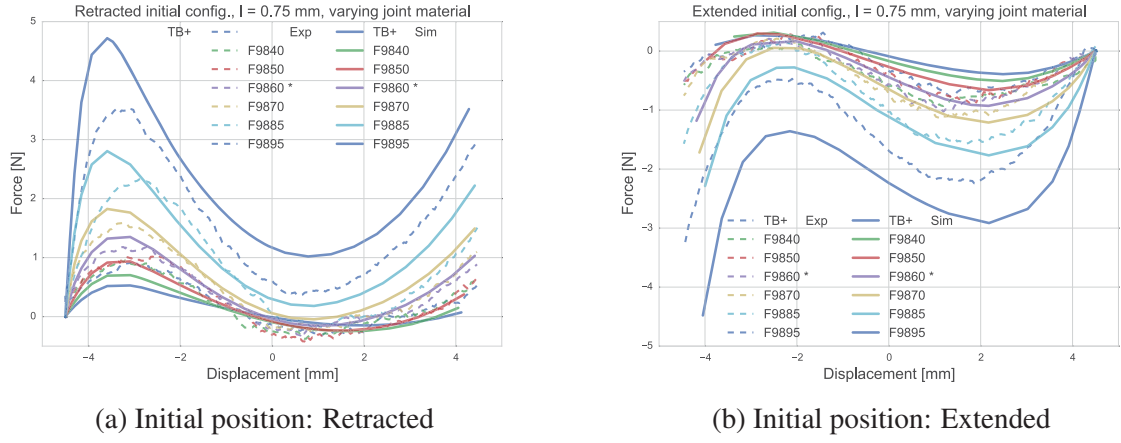


Figure 9: Force-displacement behavior from experiments and simulation with fixed joint length and varying joint material stiffness, * denotes the benchmark configuration

experimental results. In the horizontal axis are the specimens numbered according to Table 3. On the vertical axis is the peak force attained before snap-through occurs in each specimen. Both the retracted and the extended states are shown.

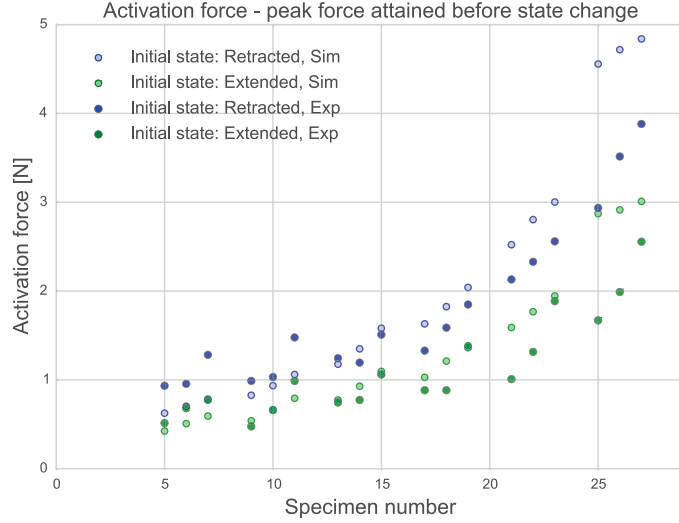


Figure 10: Activation force of each specimen - simulation and experimental results

Table 3: Specimen number and corresponding joint length and material

	1.0 mm	0.75 mm	0.50 mm
TB+	1	2	3
F9840	5	6	7
F9850	9	10	11
F9860	13	14	15
F9870	17	18	19
F9885	21	22	23
F9895	25	26	27

With the retracted specimens, an activation force ranging from 0.50 N to 5.0 N can be achieved. With the extended specimens, the activation force range is 0.25 to 3.5 N. Simulation of the activation force is able to predict experimental results with confidence, with the highest accuracy in the mid-range; simulation underestimates the activation force of actuator units using softer joint materials and overestimates the activation force of actuator units using stiffer joint materials.

Discussion

A unit actuator design leveraging different material stiffness fabricated using a multi-material 3D printer is proposed. The design is built on the idealized Von Mises Truss model where two truss members are connected by three pins, and is an improvement over the design proposed by Schioler and Pellegrino [3] in terms of overall size and stroke length to half span ratio. The stroke length over span of 100 % is significantly larger than comparable designs, Restrepo et al. [15] achieved a stroke ratio of 16 % with an Euler buckling based bistability. Schioler and Pellegrino's VMT based design has a stroke ratio of 29 % [3], and [23] using a similar design achieved 24 %. It is worth noting that the overall geometry of an Euler buckling based design encourages stacking as shown by Restrepo et al. [15].

The study sets out to design an actuator that is able to offer a range of activation forces without changing its overall geometry, and the proposed design demonstrates this property in the results section. Either by shortening the length of the joints, which lengthens the actual truss, or by increasing the stiffness of the joint material, the activation force increases predictably (Fig. 10). These parametric changes are made possible through a 3D printer that is able to deposit material of varying stiffness in a single fabrication. The design is dimensioned so that it can be stacked vertically, where the bracket of the actuator above serves at the pin of the actuator below.

A number of shortcomings are noted as well. The discrepancies between the theory and the simulation models lie largely in three aspects, completeness of the material characterization, the asymmetrical buckling behavior and accuracy of the simulation results (i.e. differences in the forces between the curves in Fig. 7). Each is discussed in turn. One, each digital material undergoes tensile testing only; the compressive behavior is assumed to be identical. Further, only one build orientation is considered. The printed plastics possess viscoelastic properties that are not addressed in material testing or in simulation. Two, the asymmetrical behavior may be caused by the following. The bracket of the actuator cannot be assumed rigid as in the idealized VMT as one may note significant bending in Fig. 11. This leads to significantly different structural behavior between the top and the bottom trusses. Three, the lack of accuracy may be explained as follows. As shown in Fig. 5C, the printed specimens do not perfectly replicate the design intent. The measured dimensions of each member is within ± 0.1 mm of the design. Due to the glossy finishing, the top surface is not flat and the edges appear to be filleted. At the material interface, significant blending of the two materials can be observed. These defects do not usually alter the performance of a large product, however they may have a pronounced effect at this scale.

Other important limitations exist primarily in the material behavior. One, all the material testing specimens are fabricated along the x-axis, whereas the unit actuators consist of members printed in all angles between x and y. This has an influence on the simulation results as the print materials are not isotropic [24]. Two, it is observed that the TB+ based materials degrade over time similar to natural rubber. This effect is controlled as the experiments are conducted on the day of fabrication. Fatigue is a major concern with such structures [21]. Its effect is controlled in this study as no specimens underwent state change prior to testing. Both time dependent effects and fatigue should be included in future studies to assess the robustness of the actuators.

Since this study focuses primarily on designing actuator configurations to provide the maxi-

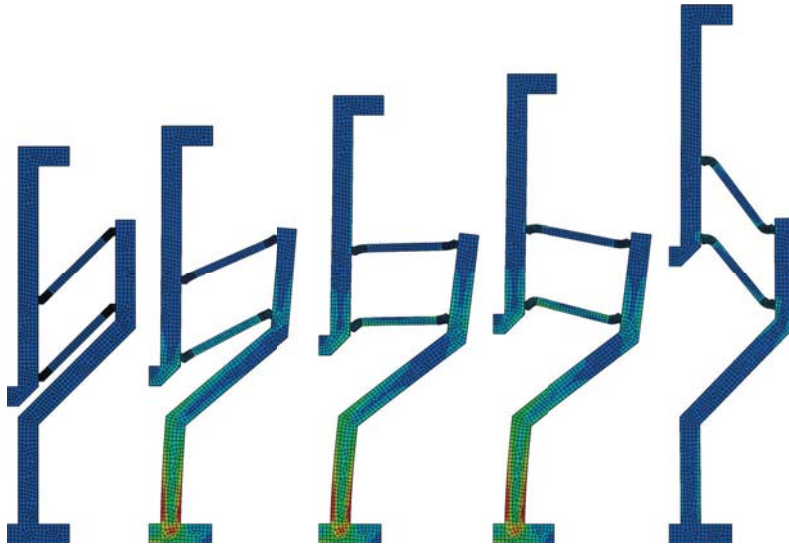


Figure 11: Deformed shape and stress distribution of an actuator in different stages of activation, note the significant bending in the bracket when the truss bars are close to being horizontal.

mum stroke length and a spectrum of activation forces, a further study is planned to vary geometric and material parameters to tailor to desired overall behavior. In particular by varying the stiffness and length of individual joints, one can plan a predictable and repeatable activation sequence.

The next logical step in this study is to incorporate such a unit actuator in designs that require many equilibrium states. Each unit may be thought of as a binary switch, and the number of stable states equal to 2^n where n is the number of units in the structure. The first step is to compound the activation forces or stroke distance in simple ways. Assuming that each actuator behaves linearly up to the point of activation, by placing two in parallel, the structure would double the force necessary to cause a state change. If one places two actuators in series, the stroke length would double. The design of multi-stable hierarchical structures based on the unit actuator proposed in this paper is presented in Chen and Shea [25].

Conclusion

A bistable actuator is designed for a multi-material 3D printer and its behavior is investigated in this work. Adapting from the Von Mises Truss model where two truss members are connected by three pin joints, the idealized joints are fabricated with materials that are much less stiff than the part material. The actuators are fabricated with a 3D printer that is able to deposit material of different stiffness values, and designed to be stackable, thereby maximizing the stroke length to half span ratio. A reduced simulation model using beam finite elements is able to predict experimental results with close agreement. Tensile testing is conducted and an experimental stress-strain curve is obtained for each material. With such constitutive models, a parametric design study of the joint length and material is done both through simulation and experimentation. By varying the joint length from 0.25 to 1.0 mm and joint material stiffness from 0.485 to 375 MPa, the actuator requires different activation forces while maintaining constant geometry and stroke length. This enables in future work tuning of actuators for design purposes.

References

- [1] Korkmaz, S., 2011. “A review of active structural control: Challenges for engineering informatics”. *Computers and Structures*, **89**(23-24), pp. 2113–2132.
- [2] Loonen, R. C. G. M., Trčka, M., Cóstola, D., and Hensen, J. L. M., 2013. “Climate adaptive building shells: State-of-the-art and future challenges”. *Renewable and Sustainable Energy Reviews*, **25**, pp. 483–493.
- [3] Schioler, T., and Pellegrino, S., 2007. “Space Frames with Multiple Stable Configurations”. *AIAA Journal*, **45**(7), pp. 1740–1747.
- [4] Leelavanichkul, S., Cherkaev, A., Adams, D. O., and Solzbacher, F., 2010. “Energy Absorption of a Helicoidal Bistable Structure”. *Journal of Mechanics of Materials and Structures*, **5**(2), pp. 305–321.
- [5] Zhang, Z., Chen, D., Wu, H., Bao, Y., and Chai, G., 2016. “Non-contact magnetic driving bioinspired Venus flytrap robot based on bistable anti-symmetric CFRP structure”. *Composite Structures*, **135**, pp. 17–22.
- [6] Ge, Q., Luo, X., Rodriguez, E. D., Zhang, X., Mather, P. T., Dunn, M. L., and Qi, H. J., 2012. “Thermomechanical behavior of shape memory elastomeric composites”. *Journal of the Mechanics and Physics of Solids*, **60**(1), pp. 67–83.
- [7] Tibbits, S., 2014. “4D Printing: Multi-Material Shape Change”. *Architectural Design: High Definition: Zero Tolerance in Design and Production*, **84**(1), pp. 116–121.
- [8] Hu, N., and Burgueño, R., 2015. “Buckling-induced smart applications: recent advances and trends”. *Smart Materials and Structures*, **24**(6), p. 063001.
- [9] Schioler, T., and Pellegrino, S., 2008. “A bistable structural element”. In IMechE, Vol. 222, pp. 2045–2051.
- [10] Pendleton, T. M., and Jensen, B. D., 2007. “Development of a Tristable Compliant Mechanism”. *12Th World Congress in Mechanism and Machine Science*.
- [11] Chen, G., Gou, Y., and Yang, L., 2010. “Research on Multistable Compliant Mechanisms: The State of the Art”. In Proceedings of the 9th International Conference on Frontiers of Design and Manufacturing, pp. 1–5.
- [12] von Mises, R., 1923. “Über die Stabilitätsprobleme der Elastizitätstheorie”. *Zeitschrift für angewandte Mathematik und Mechanik*, **3**, pp. 406–422.
- [13] Qiu, J., Lang, J. H., and Slocum, A. H., 2004. “A curved-beam bistable mechanism”. *Journal of Microelectromechanical Systems*, **13**(2), pp. 137–146.
- [14] Correa, D., Seepersad, C., and Haberman, M., 2015. “Mechanical design of negative stiffness honeycomb materials”. *Integrating Materials and Manufacturing Innovation*, **4**(1), p. 10.
- [15] Restrepo, D., Mankame, N. D., and Zavattieri, P. D., 2015. “Phase transforming cellular materials”. *Extreme Mechanics Letters*, **4**, pp. 52–60.

- [16] Han, J. S., Mueller, C., Wallrabe, U., and Korvink, J. G., 2007. “Design, Simulation, and Fabrication of a Quadstable Monolithic Mechanism With X- and Y-Directional Bistable Curved Beams”. *Journal of Mechanical Design*, **129**(11), p. 1198.
- [17] Oh, Y. S., and Kota, S., 2009. “Synthesis of multistable equilibrium compliant mechanisms using combinations of bistable mechanisms”. *Journal of Mechanical Design*, **131**(2), p. 021002.
- [18] Shan, S., Kang, S. H., Raney, J. R., Wang, P., Fang, L., Candido, F., Lewis, J. A., and Bertoldi, K., 2015. “Multistable Architected Materials for Trapping Elastic Strain Energy”. *Advanced Materials*, **27**(29), pp. 4296–4301.
- [19] Stankovic, T., Mueller, J., Egan, P., and Shea, K., 2015. “A Generalized Optimality Criteria Method for Optimization of Additively Manufactured Multimaterial Lattice Structures”. *Journal of Mechanical Design*, **137**(11), p. 111405.
- [20] Mueller, J., Shea, K., and Daraio, C., 2015. “Mechanical properties of parts fabricated with inkjet 3D printing through efficient experimental design”. *Materials & Design*, **86**, pp. 902–912.
- [21] Howell, L. L., Rao, S. S., and Midha, A., 1994. “Reliability-Based Optimal Design of a Bistable Compliant Mechanism”. *Journal of Mechanical Design*, **116**(4), pp. 1115–1121.
- [22] Cherry, B. B., Howell, L. L., and Jensen, B. D., 2008. “Evaluating three-dimensional effects on the behavior of compliant bistable micromechanisms”. *Journal of Micromechanics and Microengineering*, **18**, p. 095001.
- [23] Barbarino, S., Gandhi, F. S., and Visdeloup, R., 2013. “A Bi-Stable Von-Mises Truss for Morphing Applications Actuated Using Shape Memory Alloys”. In Proceedings of the ASME 2013 Conference on Smart Materials, Adaptive Structures and Intelligent Systems, pp. 1–11.
- [24] Mueller, J., and Shea, K., 2015. “The effect of build orientation on the mechanical properties in inkjet 3D-printing”. In International Solid Freeform Fabrication Symposium, pp. 983–992.
- [25] Chen, T., and Shea, K., 2016. “Design and Fabrication of Hierarchical Multi-Stable Structures through Multi-Material Additive Manufacturing”. In Proceedings of the ASME 2016 International Design Engineering Technical Conferences & Computers and Information in Engineering Conference.